Available online at www.sciencedirect.com
SCIENCE DIRECT
Polymer 47 (2006) 1667–1673
polymer
www.elsevier.com/locate/polymer

Crystallization and phase behavior of crystalline syndiotactic 1,2-polybutadiene/isotactic polypropylene blends in solution-cast thin films

Yong Chen, Ye Chen, Decai Yang *

State Key Laboratory of Polymer Physics and Chemistry, Changchun Institute of Applied Chemistry, Graduate School of the Chinese Academy of Sciences, Chinese Academy of Sciences, Renmin Street 5625, Changchun 130022, People's Republic of China

Received 25 August 2005; received in revised form 24 December 2005; accepted 9 January 2006
Available online 27 January 2006

Abstract

Crystallization and phase behavior in solution-cast thin films of crystalline syndiotactic 1,2-polybutadiene (*s*-1,2-PB) and isotactic polypropylene (*i*-PP) blends have been investigated by transmission electron microscopy (TEM), atomic force microscopy (AFM) and field-emission scanning electron microscopy (FESEM) techniques. Thin films of pure *s*-1,2-PB consist of parallel lamellae with the *c*-axis perpendicular to the film plane and the lateral scale in micrometer size, while those of *i*-PP are composed of cross-hatched and single-crystal-like lamellae. For the blends, TEM and AFM observations show that with addition of *i*-PP, the *s*-1,2-PB long lamellae become bended and *i*-PP itself tends to form dispersed convex regions on a continuous *s*-1,2-PB phase even when *i*-PP is the predominant component, which indicates a strong phase separation between the two polymers during film formation. FESEM micrographs of both lower and upper surfaces of the films reveal that the *s*-1,2-PB lamellae pass through *i*-PP convex regions from the bottom, i.e. the dispersed *i*-PP regions lie on the continuous *s*-1,2-PB phase. The structural development is attributed to an interplay of crystallization and phase separation of the blends in the film forming process. With solvent evaporation, *s*-1,2-PB would crystallize first forming the continuous phase, while the segregated *i*-PP phase accumulated on *s*-1,2-PB and crystallized subsequently, forming dispersed *i*-PP regions.

Keywords: Syndiotactic 1,2-polybutadiene; Isotactic polypropylene; Blends

1. Introduction

Generally, syndiotactic 1,2-polybutadiene (*s*-1,2-PB) with low crystallinity is a typical thermoplastic elastomer. By controlling 1,2-content and syndiotacticity, cystallinity of the polymer can be adjusted so as to exhibit the properties from elastomer to highly crystalline plastics [1–6]. The cystal of crystalline *s*-1,2-PB has an orthorhombic unit cell with $a=1.098$ nm, $b=0.660$ nm, and $c=0.514$ nm [2]. Although crystalline *s*-1,2-PB has been obtained for several decades, most of the research work was focused on preparation, physical properties, and application of the polymer [1–13], whereas the related morphological study was limited. Recently, we have reported the effects of crystal growth conditions on morphology of crystalline *s*-1,2-PB [14]. It was found that the *s*-1,2-PB thin films solution-cast on glycerol surface consist of lath-like lamellae with the *c*-axis perpendicular to the film plane, while spherulitic and single crystal structures can be formed in melt-crystallized thin films depending on crystallization temperatures.

As for isotactic polypropylene (*i*-PP), it is well known that there exist two types of lamellar structures in thin films, i.e. the cross-hatched and the single-crystal-like lamellae, which may coexist in one spherulite [15–18]. The cross-hatched structure is an epitaxial growth of daughter (or tangential) lamellae on mother (or radial) lamellae with their *c*-axes in the film plane and a cross-angle of ca. 80°, while the single-crystal-like lamellae, also called a lath-like structure, have the crystallographic *c*-axis vertical to the film plane.

Crystalline polymer blends, especially the crystalline/crystalline polymer blends, have received more attention in recent years [19–37]. This is not only because crystalline polymers are of prime importance from the commercial point of view, but also because the interplay between crystallization and phase separation in these systems provides new insights into the crystallization and morphology of the crystalline polymer blends, which are closely related to miscibility, crystallization condition, heat treatment, composition and property of the crystalline polymers. As a thermoplastic elastomer, it was

* Corresponding author. Tel.: +86 431 5262139; fax: +86 431 5262126.
E-mail address: dcyang@ns.ciac.jl.cn (D. Yang).

0032-3861/$ - see front matter © 2006 Elsevier Ltd. All rights reserved.
doi:10.1016/j.polymer.2006.01.008

reported that the elastomeric 1,2-PB may have some toughening effects on *i*-PP [38]. To the best of our knowledge, however, there is almost no study on the blends of highly crystalline *s*-1,2-PB and *i*-PP to date. In the present work, crystalline *s*-1,2-PB was blended with *i*-PP, and the interests are focused on crystallization and phase behavior of the two components in the blends.

2. Experimental section

2.1. Materials and sample preparation

The *i*-PP used was commercial product with melt flow index of 3.0 g/10 min. The crystallization temperature (T_c) and melting temperature (T_m) of *i*-PP were 116 and 165 °C, respectively, measured by DSC at cooling and reheating rates of 10 °C/min. The crystalline *s*-1,2-PB sample with T_c 141 °C and T_m 170 °C was found to have 87.0 mol% 1,2-content and 85.0 mol% syndiotactic regularity, based on ^{13}C NMR measurement. Weight-average molecular weight and polydispersity index (M_w/M_n) of the *s*-1,2-PB were 500,000 and 2.1, respectively.

Thin films of the *s*-1,2-PB/*i*-PP blends with different compositions were prepared by casting 0.3 wt% xylene solution of the blends on glycerol surface at 120 °C. After evaporation of the solvent, thin films were transferred onto the surface of water, and then collected on copper grids for TEM, AFM and FESEM observations. The blend powders for DSC and dynamic mechanical analysis (DMA) tests were prepared by precipitating 2.0 wt% xylene solution of the blends in cold methanol. The precipitates were dried in vacuum oven at 60 °C for 3 days.

2.2. Measurements

For TEM observations, a JEOL 1011 TEM operated at 100 kV was used. Bright-field (BF) phase contrast electron micrographs were obtained by defocus of the objective lens [39–41]. To minimize radiation damage of the polymer films caused by electron beam, thin films were carbon coated and focusing of the film was carried out on one area, and then the specimen was translated to its adjacent undamaged area and the image was taken immediately. Camera length of the electron diffraction (ED) measurement was calibrated using Au as a standard.

Topographies of upper (against air) and lower (against glycerol) surfaces of the blend films were studied by AFM and FESEM. AFM height images were obtained by a SPA-HV300 with a SPI 3800N controller (Seiko Instruments Industry Co., Ltd) in tapping mode at ambient temperature. A 150 μm scanner was selected. Probes with resonant frequency of 50–100 kHz and a spring constant of 2 N/m were used. For FESEM observation, thin films were coated with Au and an XL30 ESEM FEG scanning electron microscope was used at an accelerating voltage of 20 kV.

Variation of loss tangent (tan δ) of the blends as a function of temperature was recorded by a NETZSCH DMA-242C. Samples with dimensions of $40\times7\times1$ mm^3 were prepared from the dried precipitates which were compression-moulded at 200 °C for 3 min and then cold-pressed at room temperature. Measurements were performed from −50 to +80 °C at 3 °C/min. A tension mode was used with a frequency of 10 Hz.

DSC measurements were carried out using a Perkin–Elmer diamond differential scanning calorimeter under a protective nitrogen atmosphere, at cooling and reheating rates of 10 °C/min.

3. Results and discussion

3.1. Miscibility between s-1,2-PB and i-PP

Miscibility between amorphous portions of the two semicrystalline polymers was studied by detecting glass-transition temperatures (T_g) of the blends in DMA measurement. Fig. 1 shows the temperature spectra of tan δ for the blends at various compositions. The T_gs of neat *s*-1,2-PB and *i*-PP are ca. 35 and 13 °C, respectively. For the blends, the glass-transition peaks of predominant components (content $\geq$ 60%) in the blends can be resolved and their positions show no dependence on the blend compositions, which indicates that there is no good miscibility between the two polymers. However, the glass-transition peaks of minor components (content $\leq$ 40%) of the blends cannot be defined clearly because the peaks of the two components are too close to one another and the peak intensities are relatively weak (especially for those of *i*-PP). Even so, it seems that the glass-transition peak of *s*-1,2-PB in 40:60 (20:80) *s*-1,2-PB/*i*-PP blend shifts to lower temperature, i.e. shifting to the glass-transition temperature of *i*-PP, which implies that partial miscibility between the two components could not be eliminated.

3.2. Thermal behavior of s-1,2-PB/i-PP blends

Fig. 2 shows DSC cooling and reheating curves of the blends with various compositions at scanning rate of

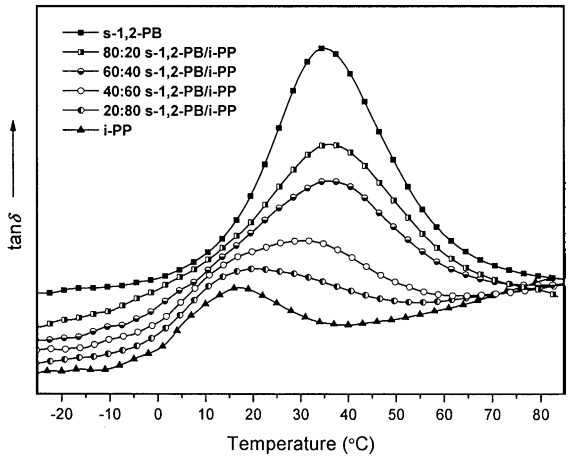

Fig. 1. Temperature spectra of tanδ at 10 Hz for *s*-1,2-PB/*i*-PP blends at various compositions.

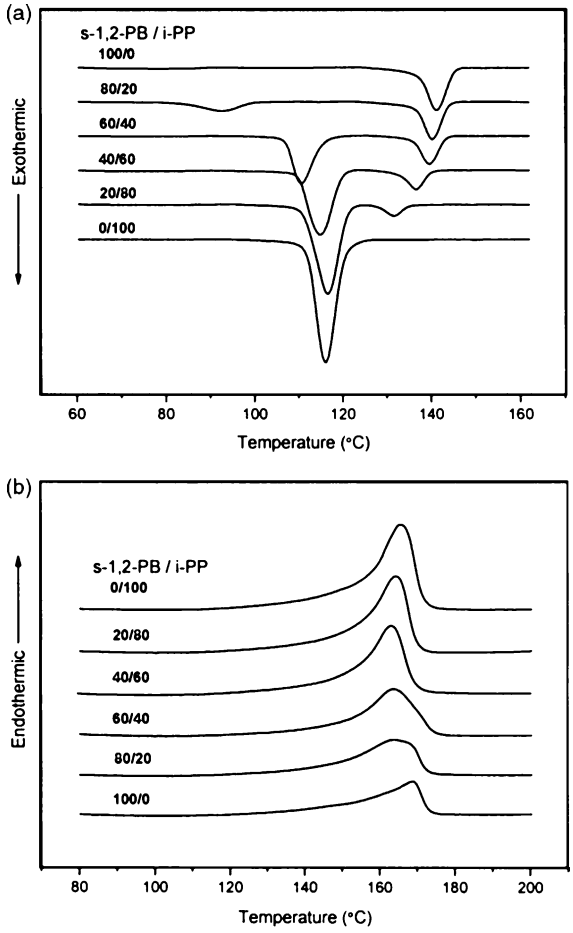

Fig. 2. DSC cooling (a) and reheating (b) curves of *s*-1,2-PB/*i*-PP blends with various compositions at a scanning rate of 10 °C/min.

10 °C/min after melting at 210 °C for 5 min. The crystallization peak temperatures of neat *s*-1,2-PB and *i*-PP are ca. 141 and 116 °C (Fig. 2(a)), respectively. For the blends, two separate exothermic peaks are observed, which correspond, respectively, to *s*-1,2-PB and *i*-PP crystallizations. It should be pointed out that the crystallization peaks of both components in the blends shift to lower temperatures compared with those of the pure components, especially for those of the minor components in the blends. The results indicate that although the miscibility between *s*-1,2-PB and *i*-PP are not so good, as revealed by the dynamic mechanical analysis, the crystallization of one component in the blends will be retarded by the other, which should be mainly attributed to kinetic or morphological effects [23]. Fig. 2(b) shows the melting behavior of the blends. As the melting temperatures of the two polymers are too close to one another, the melting peaks of the two components in blends could not be separated clearly, i.e. in the whole composition range, the blends almost exhibit a single melting peak. However, it is found that the melting temperatures of the blends decrease slightly, which implies also that the two components in blends may possess partial miscibility.

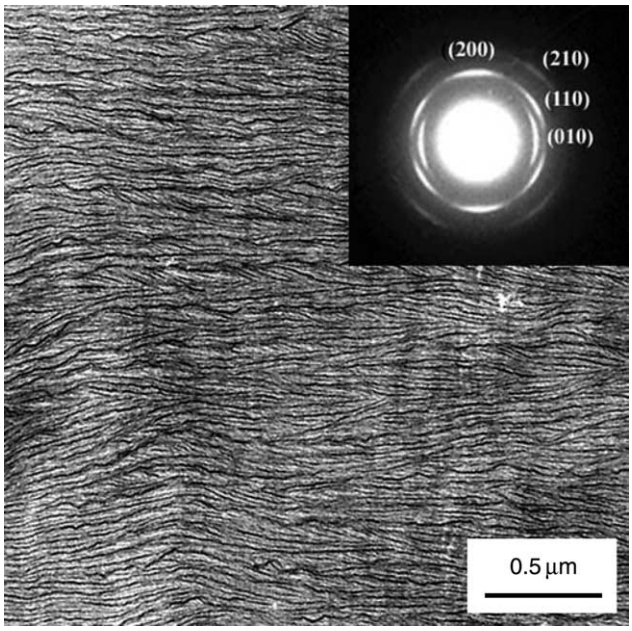

Fig. 3. BF electron micrograph and the corresponding ED pattern (inset) of *s*-1,2-PB thin film.

3.3. Crystalline structures of pure s-1,2-PB and i-PP in solution-cast thin films

Fig. 3 is BF defocus electron micrograph of solution-cast thin film of pure *s*-1,2-PB and its corresponding ED pattern (inset). The dark lines in the BF micrograph represent *s*-1,2-PB lamellae, which are almost parallel with each other and have the lateral scale in micrometer size. The (*hk0*) reflections indicate that the *c*-axis of the lamellae is perpendicular to the film plane, and the lamellar growing direction is along the crystallographic *b*-axis.

Crystalline structure of the *i*-PP thin film is shown in Fig. 4. The cross-hatched and single-crystal-like (lath-like) lamellar structures can both be observed, and the latter is confirmed by the corresponding (*hk0*) reflections (see inset). The above results are consistent with the early reports [14–18].

3.4. Morphological features of s-1,2-PB/i-PP solution-cast thin films

Figs. 5–8 show the morphologies of *s*-1,2-PB/*i*-PP blend films with different compositions. Fig. 5 is BF electron micrograph and corresponding ED pattern (inset) of 80:20 *s*-1,2-PB/*i*-PP blend film. Here, the *s*-1,2-PB-rich blend exhibits almost the same morphology as that of pure *s*-1,2-PB (compared with Fig. 3). The results indicate that the addition of small amount of *i*-PP seems to have no influence on the crystalline structure of *s*-1,2-PB. As for the minor component *i*-PP in the blend, although we could not resolve the existence of its crystalline phase by the TEM observation, it is believed that the crystallites of *i*-PP are still formed since from the DSC results (Fig. 2), a weak crystallization peak of *i*-PP at lower temperature is observed in the 80:20 *s*-1,2-PB/*i*-PP blend.

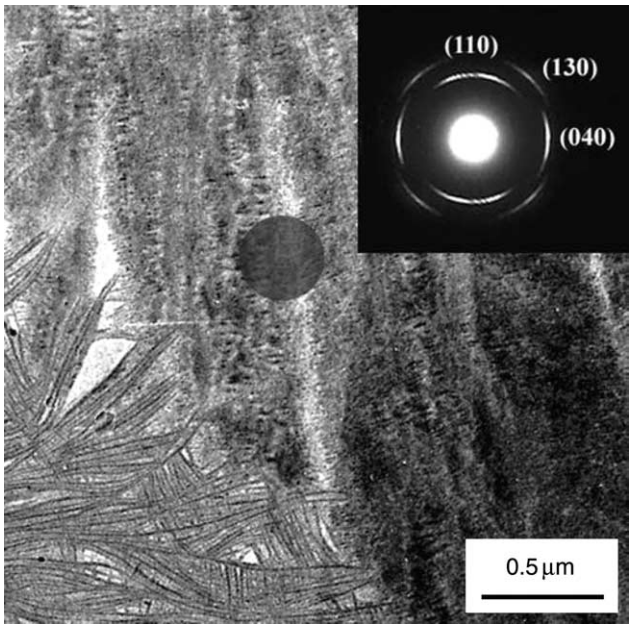

Fig. 4. BF electron micrograph of *i*-PP thin film and selected area ED pattern (inset) in the area shown by a circle. The down left and top right parts show cross-hatched and single-crystal-like lamellar structures of *i*-PP, respectively.

Fig. 6 is BF electron micrograph of 60:40 *s*-1,2-PB/*i*-PP blend film. Compared with Fig. 5, the *s*-1,2-PB long lamellae become bended, and many dispersed dark regions occur with the average size of ca. 0.2 μm. With further increase of the *i*-PP content in the blends, the bended *s*-1,2-PB lamellae exhibit random dispersion and the average dark region size increases markedly (ca. 0.5 μm), as shown in the BF electron micrograph of 30:70 *s*-1,2-PB/*i*-PP blend (Fig. 7). The selected area ED pattern of the dark regions (see inset of Fig. 7) displays two sets of reflections, i.e. relatively strong (110), (040) and (130)

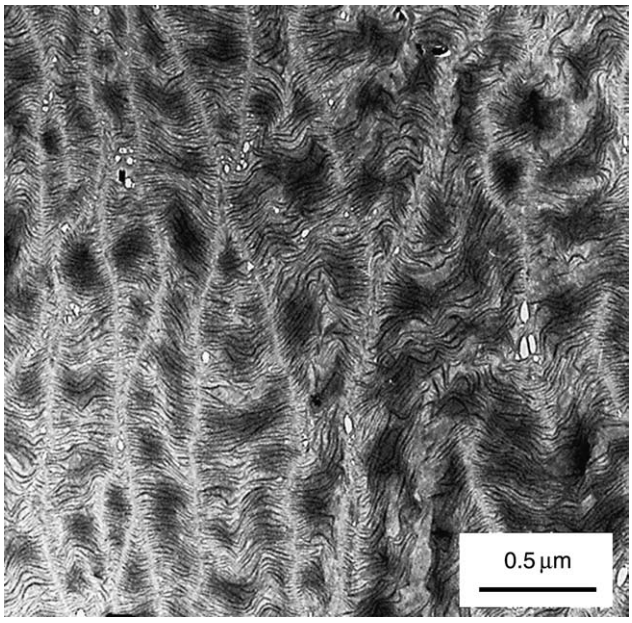

Fig. 6. BF electron micrograph of 60:40 *s*-1,2-PB/*i*-PP blend film.

reflections of *i*-PP and weak reflection rings corresponding to (210) and (110) reflections of *s*-1,2-PB, which indicates that the dark regions are coexisting phase of *i*-PP with *s*-1,2-PB. It should be pointed out that the contrast of the dark regions enhances remarkably with the increase of *i*-PP content in the blends (compared Fig. 7 with Fig. 6). Generally, the contrast in BF image is attributed to amplitude contrast, including mass thickness contrast and diffraction contrast. The stage tilting observations in electron beam (which could reduce or eliminate the diffraction contrast) indicate that the strong contrast of the dark regions mainly results from the mass thickness contrast. In other words, the dark regions represent the thick areas in films

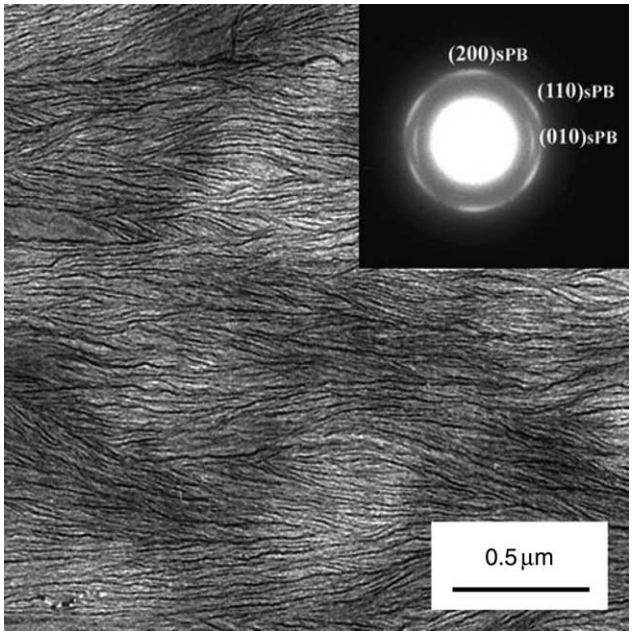

Fig. 5. BF electron micrograph and the corresponding ED pattern (inset) of 80:20 *s*-1,2-PB/*i*-PP blend film.

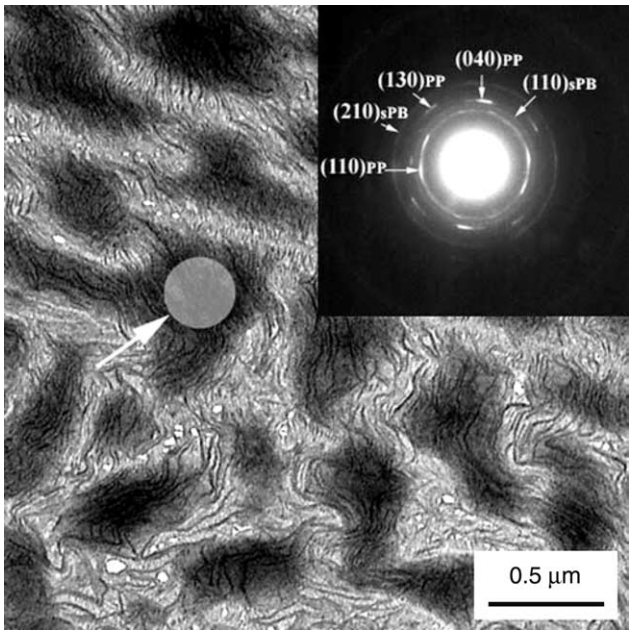

Fig. 7. BF electron micrograph of 30:70 *s*-1,2-PB/*i*-PP blend film and selected area ED pattern (inset) in the area indicated by an arrow.

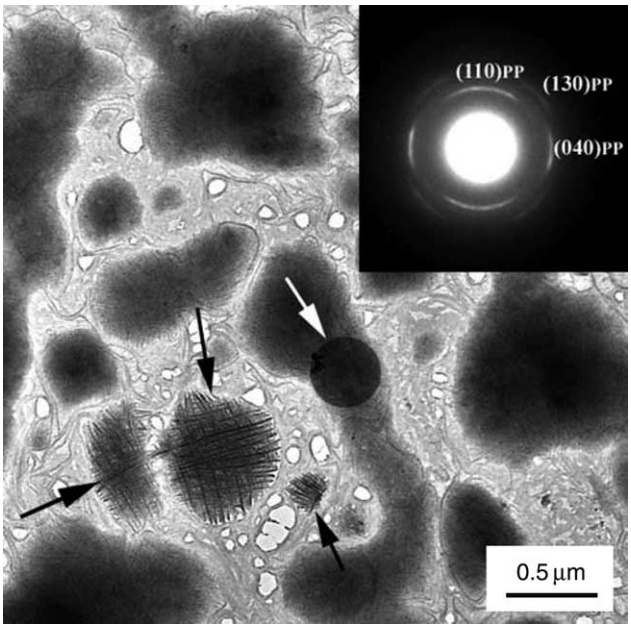

Fig. 8. BF electron micrograph of 10:90 *s*-1,2-PB/*i*-PP blend film and selected area ED pattern (inset) in the area indicated by a white arrow. The dark arrows indicate some aggregates of cross-hatched lamellae of *i*-PP.

(also see the AFM results below), which come mainly from aggregation of i-PP.

As for the 10:90 *s*-1,2-PB/*i*-PP blend film, the isolated dark regions are well-defined and become much larger (Fig. 8). Some dark regions consist of cross-hatched lamellae of i-PP (as indicated by the dark arrows), and the others should be composed of single-crystal-like *i*-PP lamellae as revealed by the selected area ED pattern (inset) in the region marked by the white arrow in Fig. 8, although the lath-like lamellae of *i*-PP in the BF image are not clear yet. Compared with Fig. 7, the number of the *s*-1,2-PB lamellae decreased markedly, but some of them seem to still penetrate the dark regions. The above results indicate that in almost the whole compositional range of the blends, *i*-PP always forms dispersed phase, even in the case that it is the predominant component in blends.

The phase-separated morphology of *s*-1,2-PB/*i*-PP blends is also shown in the surface topologic features of the blend films. Fig. 9(a) and (b) display the AFM height images of the rough surfaces of the 30:70 and 10:90 *s*-1,2-PB/*i*-PP blend films, respectively. In combination with TEM observation (Figs. 7 and 8), it is believed that the ridges and valleys in the AFM height images correspond, respectively, to the elevated *i*-PP regions and the continuous *s*-1,2-PB phase. The average height amplitude of these elevated islands of *i*-PP changes from ca. 70 nm in the 30:70 blend to ca. 100 nm in the 10:90 blend, implying a high accumulation of *i*-PP.

As illustrated by the TEM BF electron micrographs, *s*-1,2-PB lamellae look like they pass through the dispersed *i*-PP phase regions (Figs. 6 and 7). Since TEM microscopy can only provide the transmissive images of thin films, it is still difficult to determine the exact location of the *s*-1,2-PB lamellae in the elevated *i*-PP regions. Surface topologies of both sides (upper and lower surfaces) of the blend films were, therefore, studied.

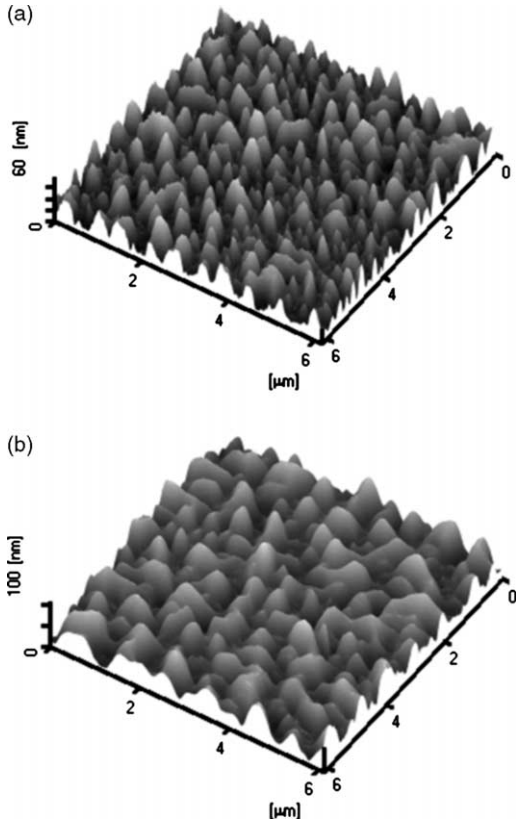

Fig. 9. AFM height images of upper surfaces of the 30:70 (a) and 10:90 (b) *s*-1,2-PB/*i*-PP blend films.

Fig. 10(a) and (b) show FESEM micrographs of the upper and lower surfaces of the 30:70 *s*-1,2-PB/*i*-PP blend film, respectively. For the upper surface (Fig. 10(a)), there exist two kinds of regions, i.e. the smooth areas which correspond to the elevated *i*-PP regions (as marked by the dark arrows), and the bright line regions which are composed of *s*-1,2-PB lamellae. Clearly, there are no *s*-1,2-PB lamellae covering on top of the *i*-PP regions. In the lower surface (Fig. 10(b)), no dispersed regions of *i*-PP can be observed, while only the bended *s*-1,2-PB lamellae are distributed in the whole film plane, forming a continuous phase.

Based on the results of both the selected area ED of dark regions in 30:70 *s*-1,2-PB/*i*-PP blend (Fig. 7) and FESEM of upper and lower surfaces of the blend films (Fig. 10), it is believed that the *s*-1,2-PB lamellae pass through *i*-PP regions from the bottom, which means the dispersed *i*-PP regions lie on a continuous phase of *s*-1,2-PB. In addition, it also reveals a fact associated with the film forming process of the blends, i.e. with solvent evaporation, *s*-1,2-PB would crystallize first and tended to form a continuous phase, while *i*-PP was segregated and accumulated on the *s*-1,2-PB phase, forming dispersed regions.

It is known that in the solution-cast processing of polymer blends, the polymers will solidify from a polymer/polymer/solvent system upon solvent evaporation. For the amorphous/amorphous polymer blends, e.g. PS/PMMA [42–46], the film solidification is a vitrification process which is associated with the T_gs of the amorphous components, while that of the

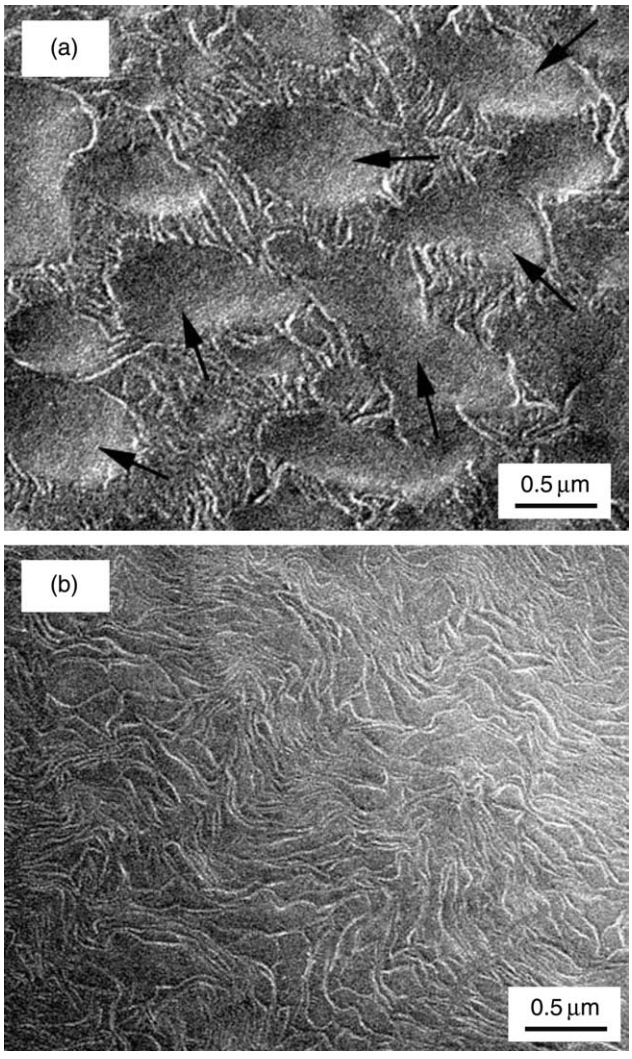

Fig. 10. FESEM micrographs of upper (a) and lower (b) surfaces of the 30:70 *s*-1,2-PB/*i*-PP blend film. The dark arrows in (a) indicate the elevated *i*-PP regions. The bending bright lines represent *s*-1,2-PB lamellae.

crystalline/crystalline polymer blends is dominated by crystallization temperature. In the case of *s*-1,2-PB/*i*-PP blends, where the film formation temperature (120 °C) is much higher than the T_gs of *s*-1,2-PB and *i*-PP, the prior crystallization of *s*-1,2-PB (which results in spreading lamellae on glycerol surface) and the bad miscibility between the two polymers (which leads to strong phase separation between *i*-PP and *s*-1,2-PB) are the main factors determining structure formation of the blends in thin films.

4. Conclusion

In this study, the morphological features of the blend thin films of two crystalline polymers, *s*-1,2-PB and *i*-PP, were revealed by a combined use of TEM, AFM and FESEM. The film forming process was discussed based on the experimental results. It is found that in almost the whole compositional range, *i*-PP always forms dispersed phase in the blends and a 'lie-on' structure can be observed in the blend films, i.e. the dispersed convex regions of *i*-PP lie on a continuous phase of *s*-1,2-PB lamellae. Based on the crystallization behavior and bad miscibility of the two polymers, the structure formation is attributed to the interplay between solvent evaporation, crystallization and phase separation of the blending system in the solution-cast process. With solvent evaporation, *s*-1,2-PB would crystallize first from the solution, forming a continuous phase, while *i*-PP was segregated and accumulated on the *s*-1,2-PB phase, resulting in dispersed convex regions.

Acknowledgements

The financial supports of the National Basic Research Program of China (2005CB623800) and Chinese Academy of Sciences (KJCX2-SW-H07) are gratefully acknowledged.

References

[1] Natta G. Makromol Chem 1955;16:213.
[2] Natta G, Corradini P. J Polym Sci 1956;20:251.
[3] Takeuchi Y, Sekimoto A, Abe M. New industrial polymers. ACS symposium series 4. Washington, DC: American Chemical Society; 1974 p. 15.
[4] Ashitaka H, Inaishi K, Ueno H, Nagasaka A. J Polym Sci, Polym Chem Ed 1983;21:1853.
[5] Ashitaka H, Jinda K, Ueno H. J Polym Sci, Polym Chem Ed 1983;21:1951.
[6] Ashitaka H, Jinda K, Ueno H. J Polym Sci, Polym Chem Ed 1983;21:1989.
[7] Obata Y, Tosaki C, Ikeyama M. Polym J 1975;7:207.
[8] Saaski T, Sunago H, Hoshikawa T. Polym Eng Sci 2003;43:629.
[9] Ricci G, Battistella M, Porri L. Macromolecules 2001;34:5766.
[10] Bertini F, Canetti M, De Chirico A, Ricci G. J Appl Polym Sci 2003;88:2737.
[11] Bertini F, Canetti M, Ricci G. J Appl Polym Sci 2004;92:1680.
[12] Ren M, Chen Q, Song J, Zhang H, Sun X, Mo Z, et al. J Polym Sci, Part B: Polym Phys 2005;43:553.
[13] Cai J, Han Y, Yuan Z, Cheng R, Wang Z, Jiang L, et al. Polym Int 2004;53:1127.
[14] Chen Y, Yang D, Hu Y, Zhang X. Cryst Growth Des 2004;4:117.
[15] Takahashi T, Mizuno H, Thomas EL. J Macromol Sci, Phys 1983;B22:425.
[16] Lotz B, Wittmann JC. J Polym Sci, Part B: Polym Phys 1986;24:1541.
[17] Olley RH, Bassett DC. Polymer 1989;30:399.
[18] Shen Y, Yang D, Feng Z. J Mater Sci 1991;26:1941.
[19] Paul DR, Bucknall CB. Polymer blends. New York: Wiley; 2000.
[20] Di Lorenzo ML. Prog Polym Sci 2003;28:663.
[21] Inaba N, Sato K, Suzuki S, Hashimoto T. Macromolecules 1986;19:1690.
[22] Inaba N, Yamada T, Suzuki S, Hashimoto T. Macromolecules 1988;21:407.
[23] Cham PM, Lee TH, Marand H. Macromolecules 1994;27:4263.
[24] Thomann R, Kressler J, Setz S, Wang C, Mülhaupt R. Polymer 1996;37:2627.
[25] Shieh YT, Lee MS, Chen SA. Polymer 2001;42:4439.
[26] Cheung YW, Stein RS. Macromolecules 1994;27:2512.
[27] Cheung YW, Stein RS, Lin JS, Wignall GD. Macromolecules 1994;27:2520.
[28] Liu LZ, Chu B, Penning JP, Manley RSJ. Macromolecules 1997;30:4398.
[29] Penning JP, Manley RSJ. Macromolecules 1996;29:77.
[30] Penning JP, Manley RSJ. Macromolecules 1996;29:84.
[31] Isayeva I, Kyu T, Manley RSJ. Polymer 1998;39:4599.
[32] Matsuba G, Shimizu K, Wang H, Wang ZG, Han CC. Polymer 2003;44:7459.
[33] Matsuba G, Shimizu K, Wang H, Wang ZG, Han CC. Polymer 2004;45:5137.
[34] Qiu ZB, Fujinami S, Komura M, Nakajima K, Ikehara T, Nishi T. Polymer 2004;45:4355.
[35] Chiu HJ, Chen HL, Lin JS. Polymer 2001;42:5749.

[36] Wignall GD, Alamo RG, Londono JD, Mandelkern L, Kim MH, Lin JS, et al. Macromolecules 2000;33:551.
[37] Chen J, Yang D. Macromolecules 2005;38:3371.
[38] Inoue T. J Appl Polym Sci 1994;54:709.
[39] Petermann J, Gleiter H. Philos Mag 1975;31:929.
[40] Miles JM, Petermann J. J Macromol Sci, Phys 1979;B16:243.
[41] Thomas EL. Encycl Polym Sci Eng 1986;5:644.
[42] Tanaka K, Takahara A, Kajiyama T. Macromolecules 1996;29:3232.
[43] Ton-That C, Shard AG, Bradley RH. Polymer 2002;43:4973.
[44] Ton-That C, Shard AG, Daley R, Bradley RH. Macromolecules 2000;33:8453.
[45] Ton-That C, Shard AG, Daley R, Bradley RH. Polymer 2001;42:1121.
[46] Walheim S, Böltau M, Mlynek J, Krausch G, Steiner U. Macromolecules 1997;30:4995.